Thermal noise from icy mirrors in gravitational wave detectors

Jessica Steinlechner [1,2] and Iain W. Martin [2,*]

[1] *Institut für Laserphysik und Zentrum für Optische Quantentechnologien, Universität Hamburg, Luruper Chaussee 149, 22761 Hamburg, Germany*

[2] *SUPA, School of Physics and Astronomy, University of Glasgow, Glasgow G12 8QQ, Scotland*

(Received 24 June 2019; published 12 August 2019)

The detection of gravitational waves has established a new and very exciting field of astronomy in the past few years. To increase the number of detections and allow observation of a wider range of sources, several future gravitational wave detectors will operate at cryogenic temperatures. Recent investigations of a mirror in one of the cryostats of the Japanese KAGRA detector showed a decrease in reflectivity due to ice growth, induced by residual water molecules moving from the warm to the cold sections of the detector's vacuum system. Based on the optical measurements made in KAGRA, in this paper we calculate the implications of an ice layer on coating thermal noise for the planned European Einstein Telescope. We find coating thermal noise to oscillate, due to periodic reflectivity changes as the ice layer grows. The average coating thermal noise increases significantly over a time of one year with a larger increase at higher temperatures.

DOI: 10.1103/PhysRevResearch.1.013008

I. INTRODUCTION

The 14th of September 2015 marks the ground-breaking event of the first detection of gravitational waves [1], almost exactly 100 years after Einstein predicted their existence [2,3]. Since then, nine more gravitational wave signals from binary black-hole mergers and one from a binary neutron-star merger have been detected [4–8] by the Advanced LIGO [9] gravitational wave detectors during their first two observing runs. The Advanced Virgo detector [10] started observing during the second run and contributed to 5 of the 11 detections [8].

Gravitational wave observatories are interferometers with perpendicular arms several kilometers in length. Their hearts are formed by large-scale, highly reflective (HR) coated mirrors. An HR coating is made of a stack of layers of two (or more) materials with alternating high and low refractive index n. The reflectivity increases with the refractive-index difference of the materials and with the number of layers. For a given number of layers, the reflectivity maximizes for an optical thickness of $n \times d_j = \lambda/4$ for each layer, in which d_j is the geometric thickness of the jth layer and λ the wavelength at which the coating is designed to be reflective. The HR coated mirrors at the ends of the gravitational wave detector arms (end test masses, ETMs) have reflectivities of about 99.9995%.

Once the advanced observatories reach their design sensitivity, coating thermal noise (CTN) from these mirrors will limit our ability to detect more gravitational waves from more distant or weaker sources. The magnitude of the *CTN amplitude spectral density*, to which a gravitational wave detector is sensitive, can be approximated by

$$x(f) = \sqrt{\frac{2k_B T}{\pi^2 f}\frac{d}{w^2}\phi\left(\frac{Y_{\mathrm{coat}}}{Y_{\mathrm{sub}}^2}+\frac{1}{Y_{\mathrm{coat}}}\right)}. \tag{1}$$

Here, k_B is the Boltzmann constant, T the mirror temperature, f the frequency, $d = \sum_j d_j$ the coating thickness, w the radius of the laser beam on the coating, and ϕ the mechanical loss of the coating. Y_{sub} and Y_{coat} are the Young's moduli of the substrate and coating materials. Following Yam *et al.* [11] we assume, in this formula, that the mechanical losses associated with bulk motion and shear motion [12] are approximately equal ($\phi_{\mathrm{bulk}} \approx \phi_{\mathrm{shear}} \approx \phi$). We follow the common convention in thermal noise modeling and assume that the mechanical loss is independent of frequency (i.e., structural damping). While the loss of amorphous coatings is not always frequency independent, the magnitude of any frequency dependence is usually small [13], and this is a good approximation for many materials [14].

Further, for simplicity, Eq. (1) neglects the effect of field penetration into the coating stack, and assumes that the Poisson's ratios σ of the coating and the substrate are 0.[1] The resulting formula [Eq. (1)] is identical to the previous description by Harry *et al.* [15] under similar approximations, and is often used for estimating CTN. However, for the CTN discussions made later in this paper, we used the more complete model by Yam *et al.* [11], which considers the different contribution of layers at different depths in the coating stack and does not neglect the Poisson ratios.

From Eq. (1) it can be seen that CTN decreases with $[(G^2+1)/Y_{\mathrm{coat}}]^{1/2}$, in which $G = Y_{\mathrm{coat}}/Y_{\mathrm{sub}}$. Therefore, it is lower for

*iain.martin@glasgow.ac.uk

[1] For a more detailed discussion of this approximation, see [15].

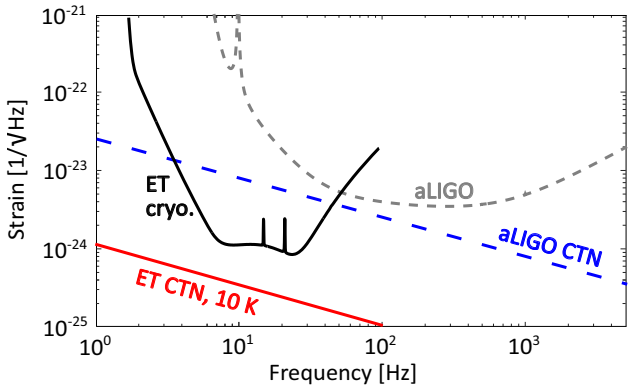

FIG. 1. Design sensitivity (gray, dashed curve) and CTN of Advanced LIGO (aLIGO) and design sensitivity and CTN at 10 K of the cryogenic Einstein Telescope (ET).

a large Y_{coat}, and in the case where $Y_{sub} > Y_{coat}$. However, as mechanical loss values of different materials generally differ much more than their Young's moduli, ϕ has proven to be the property mainly determining material selection. d and w are mainly determined by the interferometric design of the observatory. w is limited by the available mirror substrate size and the ability to coat substrates of these dimensions with suitable quality, while d depends on the required reflectivity.

The proportionality to $\sqrt{T}$ makes cooling the mirrors a very promising way forward to reduce CTN and therefore to improve sensitivity. This approach will be used in the Japanese KAGRA detector [16], which is currently under construction, in the planned European Einstein Telescope [17] and is also under consideration for future LIGO detectors.

In addition to low CTN, a low optical absorption is a highly relevant parameter for coating material selection. Heating due to absorption can cause difficulties in maintaining the low mirror temperature and lead to unwanted effects such as thermal lensing.

All these criteria make it challenging to find a coating meeting the requirements of the Einstein Telescope, which is designed to be $> 10\times$ more sensitive than current detectors. Recently, we suggested a suitable coating, using a multimaterial design which involves HfO_2, doped with SiO_2, and amorphous silicon (a-Si) in addition to the commonly used coating materials SiO_2 and Ta_2O_5 [18].

In their recent paper, Hasegawa *et al.* present observations of an ice layer growing on a mirror inside the cryogenic system of the KAGRA detector and a resulting change in the mirror's optical performance [19]. Here, we investigate the effect such an ice layer would have on CTN in the cryogenic Einstein Telescope.

II. COATING THERMAL NOISE IN THE EINSTEIN TELESCOPE

The Advanced LIGO and Advanced Virgo gravitational wave detectors operate at a wavelength of 1064 nm and at room temperature. They use fused silica (SiO_2) mirror substrates coated with SiO_2 and Ta_2O_5 doped with TiO_2. Figure 1 shows the design sensitivity of the Advanced LIGO detectors (gray, dashed curve) and the contribution of CTN (blue, dashed line). In the design study for the Einstein Telescope, an operation temperature of 10 K was suggested to reduce thermal noise at low detection frequencies [17]. The black solid curve in Fig. 1 shows the design sensitivity of the cryogenic Einstein Telescope with the design CTN at 10 K shown by the red, solid line. As higher temperatures around 20 and 120 K may also be of interest for the cryogenic Einstein Telescope, the effect of ice growth on CTN at these temperatures will also be discussed in this paper.

The mechanical loss of bulk fused silica increases by several orders of magnitude when being cooled to this temperature range [20,21], and a replacement mirror-substrate material is therefore required. For the Einstein Telescope, the use of crystalline silicon (c-Si) is planned, which shows suitably low mechanical loss at low temperatures [22,23].

As c-Si shows high optical absorption at 1064 nm, which decreases toward higher wavelengths [24,25], an increase in laser wavelength to 1550 nm is planned for the cryogenic Einstein Telescope. This results in increased CTN due to thicker coating layers. However, the larger Young's modulus of c-Si compared to fused silica has the inverse effect. A planned increase in laser beam diameter by a factor of 1.5 compared to Advanced LIGO is another factor reducing CTN.

The mechanical losses of the currently used coating materials SiO_2 and Ta_2O_5 have been observed to increase at low temperatures compared to their room-temperature values as shown in Table I [26–28], resulting in less reduction in CTN than would be obtained from the temperature decrease alone.

In summary, all these factors (the favorable increase in Y and w and reduction in T, and the unfavorable increase in d and ϕ) would result in CTN being about a factor of 2 above the Einstein Telescope requirement (the red line in Fig. 1).

TABLE I. Material parameters for thermal-noise calculations. The heat treatment temperatures and sources of the loss values are explained in detail in the Appendix. It should be noted that some of the loss values for ice are based on extrapolation from directly measured numbers.

	SiO_2	Ta_2O_5	a-Si	SiO_2:HfO_2	aH_2O
Young's modulus Y (GPa)	72 [35]	140 [35]	147 [36]	180 [37]	3.64 [38]
Refractive index n at 1550 nm	1.45 [39]	2.05 [40]	3.48 [41]	1.91 [37]	1.26[a] [19]
Mechanical loss $\phi \times 10^{-4}$ at different temperatures					
300 K	0.46 [42]	2.3 [32]	0.17 [29]		
120 K	4.8 [43]	5.7 [44]	$\leqslant$0.17 [29]	5.7 [18]	14 [45] (4.7)
20 K	9.2 [43]	5.6 [44]	$\leqslant$0.17 [29]	3.5 [18]	10 (1) [38]
10 K	8.5 [43]	5 [44]	$\leqslant$0.17 [29]	3.7 [18]	7 (1) [38]

[a]For 1064 nm.

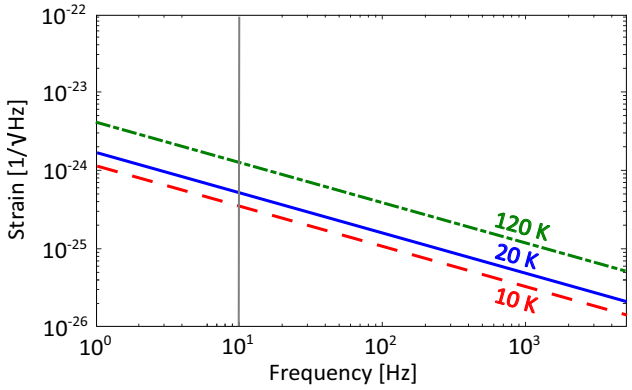

FIG. 2. CTN of the multimaterial coating presented in [18] when used for all four of the detectors arm-cavitiy mirrors, at temperatures of 10 K (bottom, red line), 20 K (middle, blue line), and 120 K (top, green line). The 10-K line is identical to the red line in Fig. 1. The vertical, gray line marks the reference frequency of 10 Hz discussed throughout this paper.

To match the CTN design of the Einstein Telescope, a change in coating materials is required. The requirement that the optical absorption is <5 ppm makes development of suitable materials even more challenging. Materials with low mechanical loss such as *a*-Si [29,30] and silicon nitride (SiN) [30,31] are promising, but show too high optical absorption. Different options for doping low-absorbing Ta_2O_5 are also under investigation [32,33], but so far could not match the thermal-noise requirements. Combining low-absorbing SiO_2 and Ta_2O_5 with low-loss *a*-Si and SiO_2:HfO_2 in a multimaterial design [11,34] is so far the only option using amorphous materials to meet both the optical and thermal-noise requirements at 10 K stated in the Einstein Telescope Design Study [17,18].

Throughout this paper, we will discuss CTN using the example of this multimaterial coating. Figure 2 shows CTN for this coating at temperatures of 10 K (red, bottom line, identical with the red line in Fig. 1), 20 K (blue, middle line), and 120 K (green, top line). Mechanical losses and Young's moduli used for calculations are shown in Table I. The effect of an ice layer can be different when growing on a different coating with similar thermal noise. However, very likely the trends shown here will be representative for other coatings.

III. COATING THERMAL NOISE OF ICE

In this section we discuss the effect an ice layer would have on CTN of the mirrors in the Einstein Telescope.

A. Ice growth on cryogenic mirrors

In their paper, Hasegawa *et al.* present observations of an ice layer growing on a cryogenic mirror in the Japanese KAGRA detector [19]. The ice grows due to the flow of molecules from the room-temperature parts of the vacuum system to the cryogenic vacuum ducts where the test masses are located, where they are adsorbed onto the cold mirror surface. The residual gas molecules were identified with a mass spectrometer to be mainly H_2O, along with O and OH, which can be generated from H_2O.

The reflectivity of the mirror in KAGRA changed periodically as the ice layer grew through multiples of quarter-wavelengths in optical thickness. In addition, there was a long-term decreasing trend in reflectivity due to optical absorption in the ice layer. As a result, the circulating laser power in the interferometer decreased over time, with an oscillation superimposed on top of this decrease from the periodic reflectivity change. A change in power affects the detector sensitivity differently at different detection frequencies as explained in detail by Hasegawa *et al.* In general, a power decrease results in a shot-noise increase at high frequencies, while at low frequencies, at which also CTN is a significant noise source, radiation pressure noise decreases.

By monitoring the optical performance of the mirror, Hasegawa *et al.* observed a continuous layer growth over several weeks and extrapolated to the expected effect on the detector due to that additional, growing ice layer over a year. They conclude a growth rate of (27 ± 2) nm/day for a mirror temperature of 47 K. They also present a theoretical model for the growth rate of the ice layer. To obtain the conductance of the complex vacuum system, they use a Monte Carlo simulation. The resulting growth rate η of the ice layer is 42 nm/day at 47 K. The calculations we want to make here for the Einstein Telescope will be based on the experimentally obtained growth rate in KAGRA of $\eta = (27 \pm 2)$ nm/day.

Here, we use literature values for the temperature-dependent mechanical loss of ice for calculating CTN. The material parameters were taken from [38] (see Table I) where the mechanical loss of ice is discussed in detail for different growth temperatures. More detail about the losses we chose to use in our calculations can be found in the Appendix of this paper. We find that an ice layer growing at the rate observed in KAGRA results in a significant increase in CTN dominated by the ice after only a few days of growth. The increasing trend of CTN due to ice is also superimposed by an oscillation, which is caused by the changing light field in the ice layer and amplified by the low Young's modulus of ice. In the following sections, we discuss these two effects in detail.

B. Oscillation of coating thermal noise due to ice growth

In a first-order approximation, coating thermal noise increases continuously with the coating thickness as shown by Eq. (1). However, when looking at a more detailed description of coating thermal noise, we find that layers show different contributions to the total coating thermal noise depending on their position in the coating stack and on their exact optical thickness, as the light field inside the coating changes due to interference effects [12,46–48]. Due to the continuous growth, the thermal-noise contribution of the layer oscillates, the maxima (and minima) separated by an optical thickness of a half-wavelength ($n \times d_1 = \lambda/2$).

A more detailed description of coating thermal noise is given by [11]

$$S_x(f) = \frac{2k_BT}{\pi^2 f}\frac{1}{w^2}\frac{1-\sigma_{\rm sub}-2\sigma_{\rm sub}^2}{Y_{\rm sub}}\sum_j b_j d_j \phi_j \,. \qquad (2)$$

b_j is a weighting factor described by

$$b_j = \frac{1}{1-\sigma_j}\left[\underbrace{\left(1 - n_j \frac{\partial\theta_{\text{coat}}}{\partial\theta_j}\right)^2}_{\text{A}} \underbrace{\frac{Y_{\text{sub}}}{Y_j}}_{\text{B}} + \underbrace{(1-2\sigma_j)\frac{Y_j}{Y_{\text{sub}}}}_{\text{C}}\right] \quad (3)$$

for $\sigma_j \approx \sigma_{\text{sub}}$. The index j refers to the material parameters defined in Eq. (1) for the jth layer in the coating (starting from the outermost layer). The index sub refers to the substrate material parameters.

The second term of Eq. (3), marked as term C, describes the effect of coating thermal stresses driving the coating-to-substrate interface [12]. This term remains constant as the ice layer grows. The first term of Eq. (3), given by $A \times B$, describes thermal noise arising from fluctuations in coating thickness. This is composed of two effects: a fluctuation in a layer changing (1) the optical thickness of this layer, and (2) the position of the front surface of the mirror.[2] These two effects work in opposite directions and partly compensate. The first effect leads to fluctuations in the round-trip phase θ_j within the jth coating layer. The term $\partial\theta_{\text{coat}}/\partial\theta_j$ describes the sensitivity of the total coating phase θ_{coat} to these fluctuations. The magnitude of $\partial\theta_{\text{coat}}/\partial\theta_j$ is proportional to the peak light-field intensity in the jth layer. As in HR coatings, the light field reduces with each double layer, the first effect is smaller for layers positioned further down in the coating. The second effect is independent of the layer position. Consequently, in lower layers, the first effect compensates less for the second effect and results in a stronger contribution of these layers to b_j, and therefore to the overall coating thermal noise. In the case of a growing ice layer, the coating phase sensitivity term oscillates due to the changing electric field intensity in the layer.[3]

Figure 3 shows the different components of Eq. (3) for a better visualization of their contributions. In addition to the case of a growing ice layer, a SiO_2 layer with identical optical thickness is shown for comparison. Figure 3(a) shows the coating phase sensitivity $\partial\theta_{\text{coat}}/\partial\theta_j$ (upper two curves), which oscillates with a period of $\lambda/2$. The amplitude of this oscillation, which is proportional to the peak electric field intensity in the layer, is slightly bigger for SiO_2 than for ice due to the higher refractive index. The two bottom curves in Fig. 3(a) show the part of Eq. (3) labeled A. The curves are still very similar for the two materials. Figure 3(b) shows the contributions of the oscillation term $A \times B$ and the constant term C to the total weighting factor b_j for SiO_2. Figure 3(c) shows the same for ice. (Note the different y axis.) It can be seen that the ratio of the Young's moduli B causes the oscillation of the ice to be much stronger than for SiO_2 due to the very small Young's modulus of ice. The second effect of this small Young's modulus is the C term being significantly smaller for ice than for SiO_2.

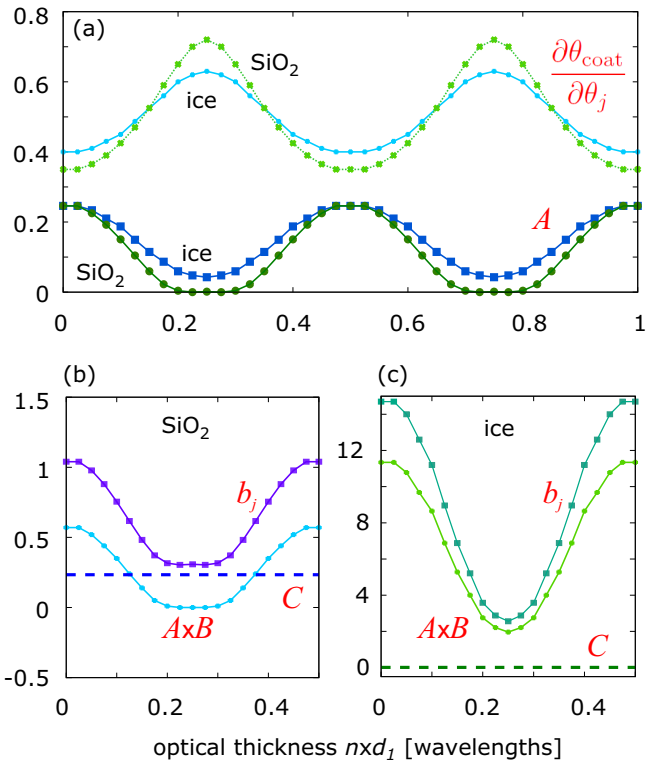

FIG. 3. Different components of Eq. (3). (a) Shows the coating phase sensitivity (two top curves) with increasing thickness for an ice layer on top of an ETM coating and a SiO_2 layer on top of the same coating. The two bottom curves show the A term for both materials. (b) Shows the contributions of the oscillation term $A \times B$ and the constant term C to the weighting term b_j for SiO_2. (c) Shows the equivalent terms for ice. (Note the different y axis.)

To illustrate the effect of different material properties of the thermal-noise oscillation, it is instructive to imagine three cases of a material growing on top of an HR stack: ice, SiO_2, and a material with the Young's modulus of SiO_2 and all other properties identical to those of ice. Figure 4 shows coating thermal noise of an ETM coating calculated using Eq. (2) as a

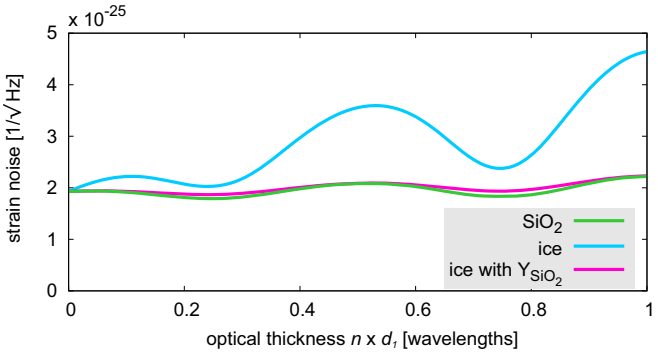

FIG. 4. CTN of an ETM coating at 10 K and a reference frequency of 10 Hz. The x axis shows the optical thickness $n \times l$ of a top layer in units of wavelengths (λ). The green, bottom curve shows CTN for a cap layer made of SiO_2 and the blue, top curve for a top layer made of ice. When assuming a Young's modulus identical to SiO_2 for ice, the oscillation gets significantly weaker as shown by the pink curve (almost identical to the bottom curve for SiO_2).

[2]In the simplified description of coating thermal noise [12,15] [see Eq. (1)], only the first effect is considered. Here, the penetration of the light field into the coating is also taken into account.

[3]While the reflectivity of the ETM changes only insignificantly (<1%) as the ice layer grows on top, the amplitude of the light field within the ice layer changes by about 60% between the minimum (for multiples of $\lambda/2$) and the maximum (for uneven multiples of $\lambda/4$).

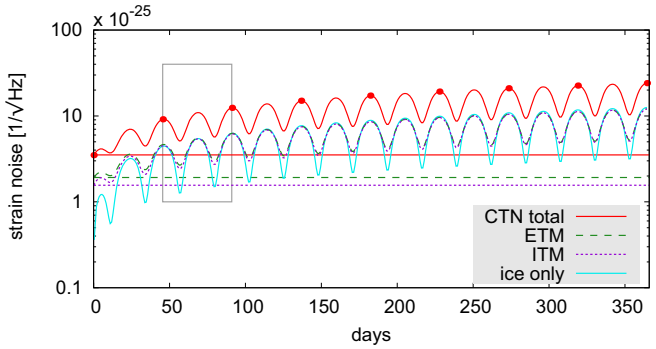

FIG. 5. Constant lines: CTN of the multimaterial coating presented in [18], separately for the ITM (bottom) and the ETM (middle), and when used for all four of the detectors arm-cavity mirrors (top), at a temperature of 10 K and a reference frequency of 10 Hz. Oscillating curves: CTN of an ice layer only when growing on a *c*-Si substrate (bottom), separately on an ITM and an ETM (middle, almost identical) and total detector CTN (all four arm-cavity mirrors, top). Red dots on the total detector CTN mark thicknesses of ice at which $n \times d_1$ is an integer multiple of a full wavelength $\lambda (= 1550\ \text{nm})$.

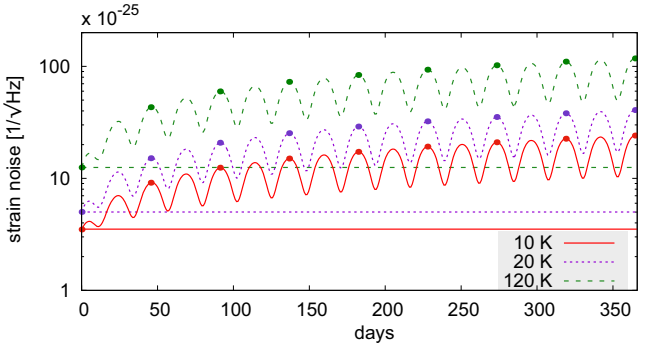

FIG. 6. Total detector CTN over one year at a reference frequency of 10 Hz at temperatures of 10 K (red, solid line), 20 K (blue, dotted line), and 120 K (green, dashed line). The oscillating curves show CTN with an ice layer growing on the mirrors, while the constant lines show CTN without ice. The 10-K curve and line are identical to the red curve and line in Fig. 5. Points on the oscillation represent thicknesses of ice at which $n \times d_1$ is an integer multiple of λ.

function of the thickness of the first layer. When the first layer is ice, a large amplitude of thermal noise oscillation is seen (blue, top line). The overall increasing trend in thermal noise arises from the increasing d [see Eq. (2)]. Next we consider the top layer to be made of SiO_2 (green, bottom line), as an example of well-known amorphous coating material with a more typical Young's modulus than ice. In this case, the oscillation amplitude is much smaller. This reduced amplitude is almost entirely due to the higher Young's modulus of silica compared to ice. This is shown by the pink line, which shows the effect for an imaginary material with the Young's modulus of SiO_2, but with all other properties identical to those of ice. This change in Young's modulus from the extremely low value of ice to a value closer to that of the substrate has an almost identical effect to that of an SiO_2 layer, with only small differences caused by a slightly different n and ϕ (see Table I).

C. Increase of coating thermal noise with time

The Einstein Telescope will have arm cavities with input test masses (ITMs) of reflectivity $R \approx 99.3\%$ and ETMs of $R \approx 99.9995\%$. The total CTN of the detector is given by $[2 \times (\text{CTN}_{\text{ETM}}{}^2 + \text{CTN}_{\text{ITM}}{}^2)]^{1/2}$, arising from two of each type of mirror. This total CTN is shown in Fig. 5 as a function of time at 10 K (constant, solid red line) for a reference frequency of 10 Hz (marked by the perpendicular, thick gray line in Fig. 2). The two bottom lines show CTN for the thinner ITM coating (purple, short dashes) and for the thicker ETM coating (green, long dashes). These three lines are flat as CTN is time independent.

The oscillating, blue line in Fig. 5 shows the CTN of an ice layer only[4] ($\phi_{10\,\text{K}} = 7 \times 10^{-4}$), growing on a *c*-Si mirror substrate at a rate of 27 nm/day. The oscillating green and purple dashed lines in Fig. 5 show CTN for an ETM and an ITM with a growing ice layer. The oscillation due to the ice layer dominates the shape of the (almost identical) ETM and ITM curves. The oscillating red, top curve shows CTN of the whole detector when ice grows on all four test-mass mirrors at the same rate. Red dots mark thicknesses of ice at which $n \times d_1$ is an integer multiple of a full wavelength λ; the gray rectangle marks one full layer optical thickness of ice grown. It can be observed that the oscillating curves with ice layers show significantly higher thermal noise, which increases as the ice layers grow, compared to the CTN without ice growth (flat bottom lines).

Figure 6 compares the total detector CTN including ice layers grown over one year at a reference frequency of 10 Hz at different temperatures. The red, solid line and curve (10 K) are identical to the red line and curve in Fig. 5. The blue, dotted and the green, dashed lines and curves show CTN at 20 and 120 K using losses for ice of $\phi = 10 \times 10^{-4}$ and 14×10^{-4} (see Table I). The points represent ice thicknesses for which $n \times d_1$ is an integer multiple of λ.

Table II shows the total detector CTN due to ice growing on the mirrors and the factor of CTN increase in brackets. Shown are the maximum increase during the first 30 days and during one year of detector operation, and the day at which this maximum occurs. Due to the lower growth rate, the increase in CTN is significantly lower for higher temperatures. However, the total CTN is still lowest at a temperature of 10 K.

IV. REDUCTION OF COATING THERMAL NOISE FROM ICE

In this section we will discuss ways to reduce the CTN increase occurring due to ice growth.

A. Reduction via annealing

The mechanical loss of ice reduces with annealing (see Table I). Heating the ice grown at 10 K to a temperature of 152 K can reduce the mechanical loss from $\phi = 7 \times 10^{-4}$

[4]To get an estimate of the effect of CTN of an ice layer only, we assumed lossless coating materials with Young's moduli identical to the *c*-Si substrate.

TABLE II. Total detector CTN at a reference frequency of 10 Hz with and without ice at the different temperatures discussed. Given are the maximum increase during the first 30 days and during one year of detector operation, and the day at which CTN maximizes. The maximum CTN and corresponding days are also given for a reduced ice growth rate by a factor of 50 and for annealing of the ice every 91 days.

CTN $\times 10^{-25}$ $(1/\sqrt{Hz})$		10 K	20 K	120 K
No ice		3.5	5.0	12.5
Ice (with factor of increase shown in brackets) (see Fig. 6)				
First 30 days	max	7.0 (2.0)	11.4 (2.3)	32.3 (2.6)
Day			25	
One year	max	24.1 (6.9)	40.7 (8.1)	117.8 (9.4)
Day			365	
Annealed ice (see Fig. 7 for 10 K)				
One year	max	14.4 (4.1)	22.1(4.4)	78.9 (6.3)
Day			365	
Low growth rate (see Fig. 8)				
One year	max	4.1(1.2)	6.3 (1.3)	16.7 (1.3)
Day		248	253	262

to 1×10^{-4} [38]. At 20 K, a factor of about 10 reduction in loss might be possible, while at 120 K it is a factor of 3 (see Appendix for details).

Figure 7 shows the total detector CTN at 10 K for annealing the mirrors to 152 K every 91 (≈3 months) days (dashed curve). Here, we imagine heating the cryogenic mirror up to 152 K for a few hours to reduce the loss of the ice. For comparison, filled circles mark maxima of thermal noise without annealing (identical to the red dots in Fig. 6). The horizontal line marks CTN without ice growth. With this periodic annealing, the maximum CTN increase within a year is a factor of 4.1, compared to a factor of 6.9 without annealing. Note that in this graph, we neglect the time it would take to heat up the mirror to 152 K and cool it back down to 10 K, which would mean a significant interruption to the detector's observation

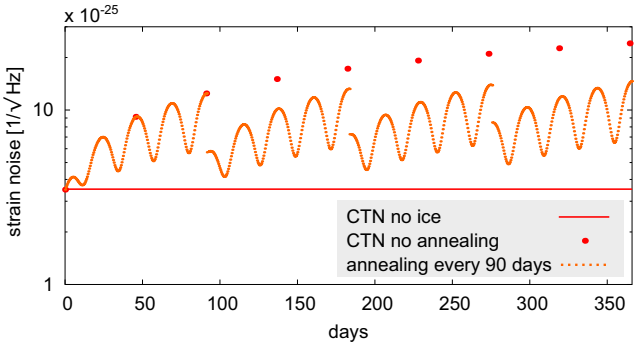

FIG. 7. Effect of annealing on the total detector CTN at 10 K and a reference frequency of 10 Hz. The red, horizontal line shows CTN without ice. The dotted orange line shows CTN with ice growth. For the first 91 days, it is identical to the red, oscillating line in Fig. 6. Every 91 days (equivalent to an ice thickness of 2 optical layers λ/n), the loss of the ice was reduced (equivalent to 152-K annealing). The red, filled circles mark thicknesses of unannealed ice for which $n \times d_1$ is an integer multiple of λ.

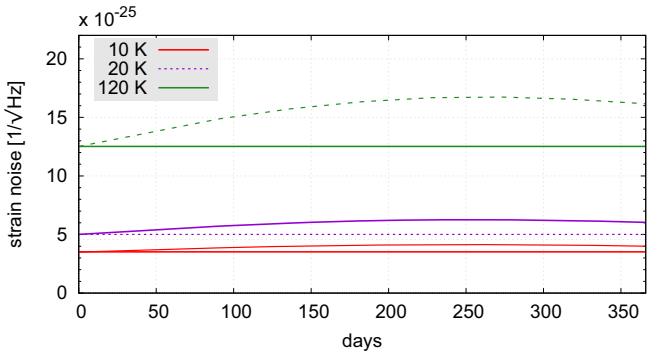

FIG. 8. Total detector CTN due to ice growth at different temperatures at a reference frequency of 10 Hz for an ice-growth rate a factor of 50 lower than in Fig. 6.

time. At 20 and at 120 K also a reduced CTN increase can be achieved from annealing (see Table II), with a higher increase due to the higher mechanical loss of ice at higher temperatures. However, for a detector operating temperature of 120 K, heating and cooling the detector for an annealing period would take significantly less time and therefore seems to be more realistic than at lower temperatures.

B. Reduction via growth-rate decrease

Another way to reduce CTN increase due to ice growth is to significantly reduce the growth rate. As stated by Hasegawa *et al.*, for KAGRA it is expected that the ice growth rate will reduce by up to a factor of 50 when reaching design pressure. Figure 8 shows the total detector CTN at different temperatures for a factor of 50 lower growth rate compared to Fig. 5. For this lower growth rate, the maximum increase in CTN within a year compared to no ice growth is also presented in Table. II. The maximum increase is a factor of 1.2 at 10 K and 1.3 at 20 and 120 K, which may be almost acceptable.

At this lower growth rate, a decrease in CTN due to annealing is still possible. Figure 9 shows CTN at 120 K for ice growth without annealing (dotted, purple line). For

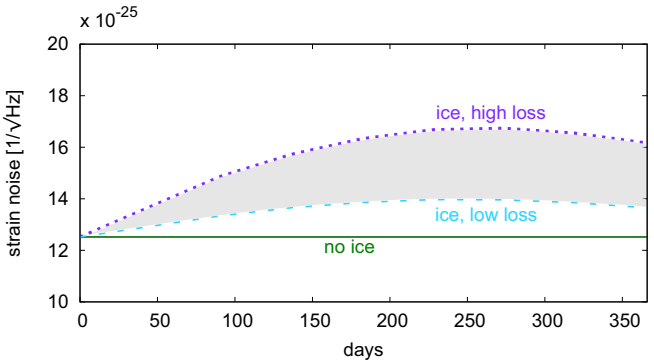

FIG. 9. Total detector CTN at 120 K without ice (solid, green line) and with ice growth (dotted, purple line) at a reference frequency of 10 Hz; these lines are identical to the 120-K data shown in Fig. 8. The dashed, light blue line shows the lower limit for CTN using the loss of annealed ice. Depending on how frequent annealing takes place, CTN will be within the gray area.

comparison, in Fig. 9 the CTN without ice growth is also shown (solid, green line). These lines are identical to Fig. 8. For very frequent annealing, CTN would converge toward the level achievable for ice with the lower, annealed loss of 4.7×10^{-4} as shown in Table I. This lower limit is given by the light blue, dashed line. Depending on the annealing frequency, which can be optimized for detector operation, CTN will be within the gray marked area.

V. SUMMARY AND DISCUSSION

We have theoretically investigated the effect an ice layer growing on the mirror surfaces could have on CTN in the Einstein Telescope based on the ice growth-rate observed in the KAGRA detector. It was found that after only a few days of growth, the ice layer will dominate CTN of the detector at operation temperatures of 10, 20, and 120 K.

CTN tends to increase as the ice layer grows on top of the coatings. This increasing trend shows an oscillation associated with the changing optical thickness of the ice layer, with a high amplitude due to the very low Young's modulus of ice. The loss of ice is higher at higher temperatures (see Table I). As a result, CTN is highest at the highest operating temperature, agreeing with the trend observed without ice growth.

For the ice growth observed in KAGRA [19] and the mechanical losses found in the literature [38,45], CTN becomes intolerably high, up to a factor of 6.9 higher than the Einstein Telescope design value at 10 K within a year of operation, and up to a factor of 9.4 at 20 K.

Annealing to about 152 K can reduce the mechanical loss of ice significantly [38,45]. Heating the mirrors to this temperature every 91 days would mean a reduced CTN increase (compared to no ice) to "only" a maximum of a factor of 4.1 at 10 K, instead of a factor of 6.9 without annealing. However, it has to be noted that a temperature increase to 152 K and the following cooling back to operating temperature would mean a significant interruption to the detector's observation ability.

Hasegawa *et al.* expect the ice growth rate to be overestimated by up to a factor of 50 as KAGRA is not yet at design pressure. Therefore, we also estimated the CTN increase for a factor of 50 lower growth rate. In this case, the maximum CTN increase within one year of operation at 10 K would be only 20% above the Einstein Telescope design value.

At a potential operating temperature of 20 K, the CTN increase due to ice is slightly higher than at 10 K. Starting the annealing procedure from a base temperature of 20 K will not lead to significantly shorter interruptions in detector operation as when starting from 10 K. Therefore, while an operating temperature of 20 K may be desirable for other reasons, there is no advantage over 10 K from an ice CTN perspective. However, at 120 K, annealing to 152 K would mean only short interruptions to detector operation.

It should be noted that all these considerations are based on growth-rate measurements in the current, not yet finalized, KAGRA configuration, and on mechanical loss measurements from the literature. While parameters have been chosen to be as close to the Einstein Telescope parameters as possible, we suggest detailed studies of the expected ice growth for the Einstein Telescope configuration as well as of the CTN of HR mirror coatings with an ice layer on top.

ACKNOWLEDGMENTS

We are grateful for financial support from STFC (Grant No. ST/N005422/1) and the University of Glasgow. I.W.M. is supported by a Royal Society Research Fellowship. We are grateful to the International Max Planck Partnership for Measurement and Observation at the Quantum Limit for support, and we thank our colleagues in the LSC and Virgo collaborations and within Scottish Universities Physics Alliance (SUPA) for their interest in this work. We would like to thank Stefan Hild for his close reading and useful questions and Hans-Herbert Otto for inspiring this work. This paper has LIGO Document number LIGO-P1900168.

APPENDIX: MECHANICAL LOSS OF ICE AND OPTICAL COATING MATERIALS

Here, we describe the origin of all of the mechanical loss values given in Table I. The heat-treatment temperature of the multimaterial coating suggested in [18] will most likely be determined by the *a*-Si layers for absorption reasons: the optical absorption of *a*-Si minimizes between 400 °C and 500 °C, varying slightly with the exact deposition procedure. The mechanical loss for the other materials was chosen to be within this temperature range. However, data for identical heat treatment temperatures were not available for all materials.

SiO_2. The loss of SiO_2 films at room temperature was taken from [42], and is for a heat-treatment temperature of 500 °C. The films were 500 nm thick and deposited by LMA (Laboratoire des Matériaux Avancés). The low-temperature loss values for SiO_2 are for a heat-treatment temperature of 450 °C [43] for a 500-nm film deposited by ATF (Advanced Thin Films).

Ta_2O_5. The loss of Ta_2O_5 at room temperature is for a Ta_2O_5 film doped with TiO_2 (14% cation concentration), heat treated at 500 °C [42]. The film was 500 nm thick and was deposited by LMA. The cryogenic loss values of Ta_2O_5 are for a heat-treatment temperature of 400 °C. Loss values of undoped Ta_2O_5 were used as no data for doped Ta_2O_5 were available for this heat-treatment temperature. The films were 500 nm in thickness and deposited by CSIRO (Commonwealth Scientific and Industrial Research Organization).

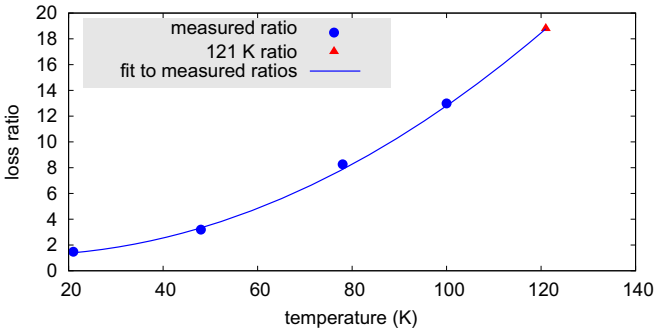

FIG. 10. Ratio of the loss of ice at deposition temperature to the loss of the same ice layer at 4 K operating temperature, as a function of deposition temperature based on data from [45]. Also shown is the fit used to extrapolate the expected ratio for a deposition temperature of 121 K, and the extrapolated ratio value.

a-Si. The loss of *a*-Si (deposited using electron cyclotron resonance ion-beam sputtering) was assumed to be 0.17×10^{-4} at all temperatures. This value is taken from [29], where it was measured at room temperature for a film deposited at 200 °C and then heat treated at 400 °C. *a*-Si films tend to show a decreasing loss on cooling below room temperature [49]. Therefore, in the absence of data for this coating at cryogenic temperatures, we have used the room-temperature value as a likely upper limit on the cryogenic loss. For the material presented in [29], the optimum heat-treatment temperature to minimize the optical absorption was 450 °C. There is evidence of a decrease of the mechanical loss of *a*-Si for slightly higher heat-treatment temperatures than 400 °C [30,49]. Therefore, an upper limit of 0.17×10^{-4} for the loss is still valid.

SiO_2:HfO_2. The loss of SiO_2:HfO_2 was taken from [18] and was measured for a 500-nm-thick coating deposited by CSIRO and heat treated at 400 °C. The SiO_2 cation concentration was 27%.

a-H_2O. Hessinger *et al.* have measured the temperature dependence of the loss of amorphous ice layers grown at different temperatures [38,45]. For all growth temperatures, a plateau in loss was observed around 4 K, with the loss tending to increase at higher measurement temperatures.

For an operating temperature of the gravitational wave detector of 20 K, we have taken the loss value for ice grown at 21 K from Fig. 10 in [38]. No data were available for ice grown at 10 K. Therefore, we have used the loss value for a growth temperature of 21 K (which was the closest to 10 K that was available in [38]), measured at 10-K operating temperature.

There are no measurements of the loss of ice grown at ∼120 K in [38]. However, for ice layers grown at other temperatures, the ratio of the losses at deposition temperature and at 4 K was found to increase with deposition temperature. A fit to this relationship, shown in Fig. 10, was used to estimate the loss of ice grown at ∼120 K.

For all three temperatures, a loss decrease from annealing can be estimated. For 20 K, the effect has directly been measured [38]. We assume an identical loss as an upper limit at 10 K. For 120 K, a factor of 3 reduction due to annealing near deposition temperature was estimated from the data in [38].

[1] B. P. Abbott, R. Abbott, T. D. Abbott, M. R. Abernathy, F. Acernese, K. Ackley, C. Adams, T. Adams, P. Addesso, R. X. Adhikari *et al.*, Observation of Gravitational Waves from a Binary Black Hole Merger, Phys. Rev. Lett. **116**, 061102 (2016).

[2] A. Einstein, Approximative integration of the field equations of gravitation, Sitzungsber. Preuss. Akad. Wiss. Berlin **1916**, 688 (1916).

[3] A. Einstein, Über Gravitationswellen, Sitzungsber. Preuss. Akad. Wiss. Berlin **1918**, 154 (1918).

[4] B. P. Abbott, R. Abbott, T. D. Abbott, M. R. Abernathy, F. Acernese, K. Ackley, C. Adams, T. Adams, P. Addesso, R. X. Adhikari *et al.*, GW151226: Observation of Gravitational Waves from a 22-Solar-Mass Binary Black Hole Coalescence, Phys. Rev. Lett. **116**, 241103 (2016).

[5] B. P. Abbott, R. Abbott, T. D. Abbott, M. R. Abernathy, F. Acernese, K. Ackley, C. Adams, T. Adams, P. Addesso, R. X. Adhikari *et al.*, GW170104: Observation of a 50-Solar-Mass Binary Black Hole Coalescence at Redshift 0.2, Phys. Rev. Lett. **118**, 221101 (2017).

[6] B. P. Abbott, R. Abbott, T. D. Abbott, M. R. Abernathy, F. Acernese, K. Ackley, C. Adams, T. Adams, P. Addesso, R. X. Adhikari *et al.*, GW170814: A Three-Detector Observation of Gravitational Waves from a Binary Black Hole Coalescence, Phys. Rev. Lett. **119**, 141101 (2017).

[7] B. P. Abbott, R. Abbott, T. D. Abbott, M. R. Abernathy, F. Acernese, K. Ackley, C. Adams, T. Adams, P. Addesso, R. X. Adhikari *et al.*, GW170817: Observation of Gravitational Waves from a Binary Neutron Star Inspiral, Phys. Rev. Lett. **119**, 161101 (2017).

[8] B. P. Abbott, R. Abbott, T. D. Abbott, S. Abraham, F. Acernese, K. Ackley, C. Adams, R. X. Adhikari, V. B. Adya, C. Affeldt *et al.* (The LIGO Scientific and Virgo Collaborations), GWTC-1: A Gravitational-Wave Transient Catalog of Compact Binary Mergers Observed by LIGO and Virgo during the First and Second Observing Runs, arXiv:1811.12907 [Phys. Rev. X (to be published)].

[9] J. Aasi, B. P. Abbott, R. Abbott, T. Abbott, M. R. Abernathy, K. Ackley, C. Adams, T. Adams, P. Addesso, R. X. Adhikari *et al.*, Advanced LIGO, Classical Quantum Gravity **32**, 074001 (2015).

[10] F. Acernese, M. Agathos, K. Agatsuma, D. Aisa, N. Allemandou, A. Allocca, J. Amarni, P. Astone, G. Balestri, G. Ballardin *et al.*, Advanced Virgo: a 2nd generation interferometric gravitational wave detector, Classical Quantum Gravity **32**, 024001 (2015).

[11] W. Yam, S. Gras, and M. Evans, Multimaterial coatings with reduced thermal, Phys. Rev. D **91**, 042002 (2015).

[12] T. Hong, H. Yang, E. K. Gustafson, R. X. Adhikari, and Y. Chen, Brownian thermal noise in multilayer coated mirrors, Phys. Rev. D **87**, 082001 (2013).

[13] G. M. Harry, M. R. Abernathy, A. E. Becerra-Toledo, H. Armandula, E. Black, K. Dooley, M. Eichenfield, C. Nwabugwu, A. Villar, D. R. M. Crooks, G. Cagnoli, J. Hough, C. R. How, I. MacLaren, P. Murray, S. Reid, S. Rowan, P. H. Sneddon, M. M. Fejer, R. Route *et al.*, Titania-doped tantala/silica coatings for gravitational-wave detection, Classical Quantum Gravity **24**, 405 (2007).

[14] P. R. Saulson, Thermal noise in mechanical experiments, Phys. Rev. D **42**, 2437 (1990).

[15] G. M. Harry, A. M. Gretarsson, P. R. Saulson, S. E. Kittelberger, S. D. Penn, W. J. Startin, S. Rowan, M. M. Fejer, D. R. M. Crooks, G. Cagnoli, J. Hough, and N. Nakagawa, Thermal noise in interferometric gravitational wave detectors due to dielectric optical coatings, Classical Quantum Gravity **19**, 897 (2002).

[16] K. Somiya for the KAGRA collaboration, Detector configuration of KAGRA-the Japanese cryogenic gravitational-wave detector, Classical Quantum Gravity **29**, 124007 (2012).

[17] M. Abernathy, F. Acernese, P. Ajith, B. Allen, P. Amaro-Seoane, N. Andersson, S. Aoudia, P. Astone, B. Krishnan, L. Barack *et al.*, Einstein gravitational wave Telescope (ET) conceptual design study, ET-0106C-10, https://tds.ego-gw.it/ql/?c=7954 (2010).

[18] K. Craig, J. Steinlechner, P. G. Murray, A. S. Bell, R. Birney, K. Haughian, J. Hough, I. MacLaren, S. Penn, S. Reid, R. Robie, S. Rowan, and I. W. Martin, Mirror Coating Solution for the Cryogenic Einstein Telescope, Phys. Rev. Lett. **122**, 231102 (2019).

[19] K. Hasegawa, T. Akutsu, N. Kimura, Y. Saito, T. Suzuki, T. Tomaru, A. Ueda, and S. Miyoki, Molecular adsorbed layer formation on cooled mirrors and its impacts on cryogenic gravitational wave telescopes, Phys. Rev. D **99**, 022003 (2019).

[20] J. W. Marx and J. M. Sivertsen, Temperature dependence of the elastic moduli and internal friction of silica and glass, J. Appl. Phys. **24**, 81 (1953).

[21] A. Schroeter, R. Nawrodt, R. Schnabel, S. Reid, I. Martin, S. Rowan, C. Schwarz, T. Koettig, R. Neubert, M. Thürk, W. Vodel, A. Tünnermann, K. Danzmann, and P. Seidel, On the mechanical quality factors of cryogenic test masses from fused silica and crystalline quartz, arXiv:0709.4359v1.

[22] D. F. McGuigan, C. C. Lam, R. Q. Gram, A. W. Hoffman, D. H. Douglass, and H. W. Gutche, Measurements of the mechanical Q of single-crystal silicon at low temperatures, J. Low Temp. Phys. **30**, 624 (1978).

[23] R. Nawrodt, A. Zimmer, T. Koettig, C. Schwarz, D. Heinert, M. Hudl, R. Neubert, M. Thürk, S. Nietzsche, W. Vodel, P. Seidel, and A. Tünnermann, High mechanical Q-factor measurements on silicon bulk samples, J. Phys.: Conf. Ser. **122**, 012008 (2008).

[24] M. J. Keevers and M. A. Green, Absorption edge of silicon from solar cell spectral response measurements, Appl. Phys. Lett. **66**, 174 (1995).

[25] J. Degallaix, R. Flaminio, D. Forest, M. Granata, C. Michel, L. Pinard, T. Bertrand, and G. Cagnoli, Bulk optical absorption of high resistivity silicon at 1550 nm, Opt. Lett. **38**, 2047 (2013).

[26] M. Granata, K. Craig, G. Cagnoli, C. Carcy, W. Cunningham, J. Degallaix, R. Flaminio, D. Forest, M. Hart, J.-S. Hennig, J. Hough, I. MacLaren, I. W. Martin, C. Michel, N. Morgado, S. Otmani, L. Pinard, and S. Rowan, Cryogenic measurements of mechanical loss of high-reflectivity coating and estimation of thermal noise, Opt. Lett. **38**, 5268 (2013).

[27] I. W. Martin, R. Nawrodt, K. Craig, C. Schwarz, R. Bassiri, G. Harry, J. Hough, S. Penn, S. Reid, R. Robie, and S. Rowan, Low temperature mechanical dissipation of an ion-beam sputtered silica film, Classical Quantum Gravity **31**, 035019 (2014).

[28] I. W. Martin *et al.*, Comparison of the temperature dependence of the mechanical dissipation in thin films of Ta_2O_5 and Ta_2O_5 doped with TiO_2, Classical Quantum Gravity **26**, 155012 (2009).

[29] R. Birney, J. Steinlechner, Z. Tornasi, S. MacFoy, D. Vine, A. S. Bell, D. Gibson, J. Hough, S. Rowan, P. Sortais, S. Sproules, S. Tait, I. W. Martin, and S. Reid, Amorphous Silicon with Extremely Low Absorption: Beating Thermal Noise in Gravitational Astronomy, Phys. Rev. Lett. **121**, 191101 (2018).

[30] J. Steinlechner, I. W. Martin, A. S. Bell, J. Hough, M. Fletcher, P. G. Murray, R. Robie, S. Rowan, and R. Schnabel, Silicon-Based Optical Mirror Coatings for Ultrahigh Precision Metrology and Sensing, Phys. Rev. Lett. **120**, 263602 (2018).

[31] H. Pan, L. Kuo, L. Chang, S. Chao, I. Martin, J. Steinlechner, and M. Fletcher, Silicon nitride and silica quarter-wave stacks for low-thermal-noise mirror coatings, Phys. Rev. D **98**, 102001 (2018).

[32] R. Flaminio, J. Franc, C. Michel, N. Morgado, L. Pinard, and B. Sassolas, A study of coating mechanical and optical losses in view of reducing mirror thermal noise in gravitational wave detectors, Classical Quantum Graity. **27**, 084030 (2010).

[33] K. Prasai, J. Jiang, A. Mishkin, B. Shyam, S. Angelova, R. Birney, D. A. Drabold, M. Fazio, E. K. Gustafson, G. Harry, S. Hoback, J. Hough, C. Lévesque, I. MacLaren, A. Markosyan, I. W. Martin, C. S. Menoni, P. G. Murray, S. Penn, S. Reid *et al.*, High Precision Detection of Change in Intermediate Range Order of Amorphous Zirconia-Doped Tantala Thin Films Due to Annealing, Phys. Rev. Lett. **123**, 045501 (2019).

[34] J. Steinlechner, I. W. Martin, C. Krueger, J. Hough, S. Rowan, and R. Schnabel, Thermal noise reduction and absorption optimisation via multi-material coatings, Phys. Rev. D **91**, 042001 (2015).

[35] M. M. Fejer, S. Rowan, G. Cagnoli, D. R. M. Crooks, A. Gretarsson, G. M. Harry, J. Hough, S. D. Penn, P. H. Sneddon, and S. P. Vyatchanin, Thermoelastic dissipation in inhomogeneous media: loss measurements and displacement noise in coated test masses for interferometric gravitational wave detectors, Phys. Rev. D **70**, 082003 (2004).

[36] M. R. Abernathy, Mechanical properties of coating materials for use in the mirrors of interferometric gravitational wave detectors, Ph.D. thesis, University of Glasgow, UK, 2012.

[37] K. Craig, Studies of the mechanical dissipation of thin films for mirrors in interferometric gravitational wave detectors, Ph.D. Thesis, University of Glasgow, UK, 2015.

[38] J. Hessinger, B. E. White Jr., and R. O. Pohl, Elastic properties of amorphous and crystalline ice films, Planet Space Sci. **44**, 937 (1996).

[39] D. B. Leviton and B. J. Frey, Temperature-dependent absolute refractive index measurements of synthetic fused silica, Proc. SPIE **6273**, 62732K (2006).

[40] J. Franc, N. Morgado, R. Flaminio, R. Nawrodt, I. Martin, L. Cunningham, A. Cumming, S. Rowan, and J. Hough, Mirror thermal noise in laser interferometer gravitational wave detectors operating at room and cryogenic temperature arXiv:0912.0107.

[41] D. T. Pierce and W. E. Spicer, Electronic structure of amorphous Si from photoemission and optical studies, Phys. Rev. B **5**, 3017 (1972).

[42] M. Granata, E. Saracco, N. Morgado, A. Cajgfinger, G. Cagnoli, J. Degallaix, V. Dolique, D. Forest, J. Franc, C. Michel, L. Pinard, and R. Flaminio, Mechanical loss in state-of-the-art amorphous optical coatings, Phys. Rev. D **93**, 012007 (2016).

[43] R. R. Robie, Characterisation of the mechanical properties of thin-film mirror coating materials for use in future interferometric gravitational wave detectors, Ph.D. thesis, University of Glasgow, UK, 2018.

[44] I. W. Martin, R. Bassiri, R. Nawrodt, M. M. Fejer, A. Gretarsson, E. Gustafson, G. Harry, J. Hough, I. MacLaren, S. Penn, S. Reid, R. Route, S. Rowan, C. Schwarz, P. Seidel, J. Scott, and A. L. Woodcraft, Effect of heat treatment on mechanical dissipation in Ta_2O_5 coatings, Classical Quantum Gravity **27**, 225020 (2010).

[45] J. Hessinger and R. O. Pohl, Annealing of amorphous ice films, J. Non-Cryst. Solids **208**, 151 (1996).

[46] M. L. Gorodetsky, Thermal noises and noise compensation in high-reflection multilayer coating, Phys. Lett. A **372**, 6813 (2008).

[47] A. Gurkovsky and S. Vyatchanin, Thermal noises and noise compensation in high-reflection multilayer coating, Phys. Lett. A **374**, 3267 (2010).

[48] N. M. Kondratiev, A. G. Gurkovsky, and M. L. Gorodetsky, Thermal noise and coating optimization in multilayer dielectric mirrors, Phys. Rev. D **84**, 022001 (2011).

[49] P. G. Murray, I. W. Martin, K. Craig, J. Hough, R. Robie, S. Rowan, M. R. Abernathy, T. Pershing, and S. Penn, Ion-beam sputtered amorphous silicon films for cryogenic precision measurement systems, Phys. Rev. D **92**, 062001 (2015).